ACS MEASUREMENT SCIENCE Au
AN OPEN ACCESS JOURNAL OF THE AMERICAN CHEMICAL SOCIETY

pubs.acs.org/measureau
Article

Activatable Multiplexed ^{19}F NMR Probes for Dynamic Monitoring of Biomarkers Associated with Cellular Senescence

Published as part of ACS Measurement Science Auspecial issue"2024 Rising Stars".

Jian Wang, Donghui Hong, Jili Li,* Linlin Wang, Yuqi Xie, Jun Da, and Yanlan Liu*

Cite This: *ACS Meas. Sci. Au* 2024, 4, 577−584

Read Online

ACCESS | Metrics & More | Article Recommendations | Supporting Information

ABSTRACT: Simultaneous detection of multiple biomarkers is crucial to achieve specific and dynamic analysis of cellular senescence, given its intrinsic high heterogeneity. Current approaches for senescence detection largely rely on fluorescence imaging, but fluorescent probes inevitably suffer from issues including autofluorescence and spectral overlap when being applied for the simultaneous detection of multiple biomarkers. Herein, we report an alternative strategy and design activatable multiplexed senoprobes based on ^{19}F NMR for dynamic monitoring of cellular senescence. Differing from previous approaches, our strategy has two unique advantages. First, this strategy utilizes the changes in the ^{19}F chemical shift as the signal output, which features by its fingerprint and quantifiable characters, thereby significantly enhancing the detection throughput toward biomarkers with minimized spectral overlapping. Second, the background signal is minimized, benefiting from the extremely low abundance of F in biological samples, and the detection accuracy can thus be improved. As a proof of concept, two activatable ^{19}F NMR molecular probes are synthesized that specially respond to two key senescence-associated biomarkers (β-gal and ROS) and have been successfully demonstrated for dynamical and quantitative assessment of the changes of these biomarkers in different cellular models of senescence, without causing obvious cytotoxicity. Owing to the flexible molecular design, this work may offer a useful platform to create diversified ^{19}F NMR senoprobes for deep understanding of cellular senescence across a wide range of aging-related diseases.

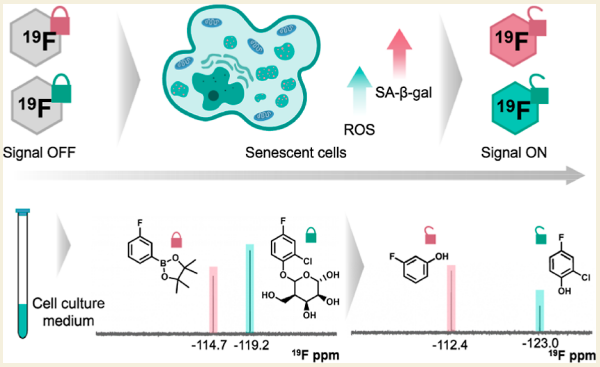

KEYWORDS: *cellular senescence, ^{19}F NMR, activatable senoprobes, biomarker analysis, multiplex detection*

Cellular senescence is a ubiquitous biological process involving permanent cell-cycle arrest in proliferating cells triggered by stresses.[1−3] Advances in cytobiology and clinicopathology have revealed that cellular senescence plays important roles in regulating various biological processes but behaves like a double-edged sword. On one hand, cellular senescence is a cellular defense mechanism responsible for preventing uncontrolled proliferation of damaged cells and cancer development and is particularly important to enhance innate immune and maintain organism homeostasis.[4−6] On the other hand, persistent accumulation of senescent cells in tissues can be maladaptive because it can ironically remodel the tissue microenvironment via the senescence-associated secretory phenotype (SASP), contributing to the development of various adverse consequences such as organ dysfunction, tumor relapse and metastasis, and aging-related diseases.[7−9] Therefore, senescent cells have been proposed as a promising target for basic studies and disease theranostics.[10,11] However, cellular senescence is a complicated biological process, demonstrating high heterogeneities in different cell sources, stimulation types, and durations, posing a great challenge for precise detection and dynamic analysis of cellular senescence and related diseases.[12]

The development of senescence probes capable of simultaneously detecting multiple senescence-associated biomarkers has been suggested as an effective way to address the above challenge and further improve the specificity compared to traditional single-marker detection approaches.[13−23] Currently, such senoprobes are largely designed based on fluorescence imaging because of the high sensitivity and spatiotemporal resolution of this technique. They can directly recognize and specifically react with senescence-associated biomarkers to generate fluorescence signal changes only in the coexistence of the biomarkers, contributing to an enhanced signal-to-background ratio and increased specificity.[24−26]

Received: July 22, 2024
Revised: August 23, 2024
Accepted: August 26, 2024
Published: August 31, 2024

https://doi.org/10.1021/acsmeasuresciau.4c00045
ACS Meas. Sci. Au 2024, 4, 577−584

Despite the great potential, these fluorescence-based detection approaches still suffer from inevitable drawbacks, including but not limited to the following aspects: (i) strong spectral overlap derived from the broad emission spectra of fluorochromes that are virtually impossible to separate into specific channels during imaging, which greatly restrict their applications in simultaneously imaging multiple senescence-associated biomarkers; (ii) severe autofluorescence interference from biological samples, hindering further improvement in the imaging accuracy; and (iii) complicated molecular design and screening to ensure good reactivity toward different targets of interest, which significantly increases the difficulty in bench-to-bedside transformation. Consequently, strategic innovations with flexible design, minimized background interference, and signal overlap are highly desirable for the simultaneous detection of different senescence biomarkers.

^{19}F nuclear magnetic resonance (NMR) spectroscopy is widely recognized as a powerful tool for simultaneous and quantitative analysis of multiple targets, owing to its many merits including broad-range and fingerprint-like chemical shifts (>350 ppm), adaptive sensitivity, and quantitative NMR signal output.[27−29] Moreover, the level of F element in organism is extremely low (<10^{-6} M and only in bone and teeth), enabling minimized background signals and interference when ^{19}F NMR is used for biological analysis. In addition, the ^{19}F chemical shift is very sensitive to the chemical environment change, making it particularly attractive to create biomarker-activatable ^{19}F NMR probes to further improve the detection specificity.[30−36] Of note, a minor difference in chemical shift (0.03 ppm) is sufficient to achieve baseline separation of two single ^{19}F resonances, which can efficiently overcome the spectral overlapping issue in optimal imaging techniques.[37−39] With these distinct features, we envisioned that constructing activatable ^{19}F NMR probes can achieve a more accurate detection of senescent cells and help to depict molecular fingerprint information in cells upon cellular senescence. Nevertheless, such investigations have remained elusive.

To this end, here we report our conceptual design of activatable multiplexed ^{19}F NMR senoprobes and demonstrate their applications in senescence detection and dynamic monitoring in different cell lines (Figure 1). As a proof-of-concept illustration, senescence-associated β-galactosidase (SA-β-Gal, the current gold-standard senescence biomarker) and ROS (a major type of SASP) are selected as the models of target, and two activatable ^{19}F NMR senoprobes have been synthesized. These two probes, namely, Gal-4-F-2-Cl and ROS-3-F, are composed of fluorine-containing moieties with distinctive ^{19}F chemical shifts and target recognition units. Upon recognition of SA-β-Gal and ROS in senescent cells, respectively, these probes would yield new chemical entities, and the ^{19}F chemical shifts of the nascent entities are substantially different from those of primary probes, enabling sensitive and readily quantitative assessment of biomarkers. More importantly, the ^{19}F chemical shifts of the initial probes and the generated new entities are remarkably separated, allowing for simultaneous analysis of SA-β-Gal and ROS in senescent cells with minimal signal overlap. The potential of these activatable multiplexed ^{19}F NMR probes for simultaneous analysis has been successfully illustrated by NMR spectroscopy analysis in various senescent models from different cell sources. Overall, we expect this work to lay the groundwork for creating an arsenal of activatable multiplexed ^{19}F NMR senoprobes due to the flexible molecular design and intrinsic multicolor-like nature of ^{19}F NMR, which we believe will empower efforts to improve the analytical capability toward senescence biomarkers and offer the future possibility to depict molecular signatures of cellular senescence for a deep understanding of its biological roles.

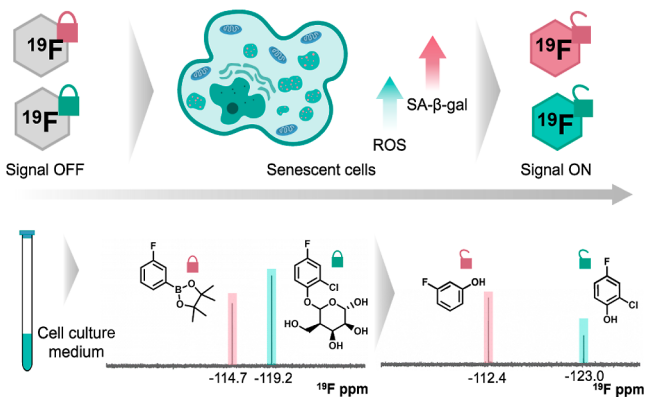

Figure 1. Schematic illustration of the design of the activatable multiplexed ^{19}F NMR probes and their mechanisms for simultaneous detection and monitoring of different senescence biomarkers.

EXPERIMENTAL SECTION

Synthesis of the Activatable Multiplexed ^{19}F NMR Probes

Detailed synthesis and characterizations of Gal-4-F-2-Cl and ROS-3-F can be found in Supporting Information.

Reactivity Studies

The reactivity of these probes was assessed by high-performance liquid chromatography (HPLC) and UV−vis absorbance spectroscopy. To investigate the reactivity of Gal-4-F-2-Cl toward β-gal, the stock solution of Gal-4-F-2-Cl in DMSO (100 mM) was dissolved in PBS (pH 7.4) containing 10% D_2O to yield a final concentration of 400 μM, followed by incubation with versus without β-gal (0.1 U/mL) at 37 °C for 3 h. HPLC was performed to monitor the changes in the absorbance at 270 nm. As a reference, HPLC profiles of free 2-chloro-4-fluorophenol (4-F-2-Cl-OH) were also collected under the same procedures. The HPLC procedures are outlined in Table S1. The reactivity of ROS-3-F to ROS was checked after incubation of ROS-3-F (400 μM) with versus without ROS (1 mM) for 3 h. Free 3-fluorophenol (3-F-OH) was also tested using the same procedures. UV−vis absorbance spectra of these two probes before and after treatment with targets were recorded by using a UV−vis spectrophotometer (Shimadzu, UV-2600i, Shanghai, China).

Establishment of Cellular Senescence Models

The human normal hepatic cell line (L-02 cells), human embryonic kidney cell line (HEK293T cells), human lung cancer cell line (A549 cells), and human prostate cancer cell line (PC-3 cells) were used as the model cells, and DOX was used as the inducer. All cell lines were cultured in RPMI 1640 supplemented with fetal bovine serum (FBS, 10%) and antibiotics (penicillin/streptavidin) (1%) at 37 °C and were cultured in a humidified atmosphere containing 5% CO_2. To induce senescence, 1.2 × 10^6 L-02, HEK293T, A549, and PC-3 cells were separately seeded into the dish and cultured in the presence of DOX (200 nM) for 4 days. The culture medium was replaced every 2 days. Afterward, the cells were cultured in a fresh medium for an additional 3 days prior to the following experiments.

In Vitro ^{19}F NMR Assay

To examine the detectability of senoprobes for senescence-associated markers in senescent cells, an in vitro ^{19}F NMR assay was performed. Briefly, senescent cells and proliferating control cells were collected by

https://doi.org/10.1021/acsmeasuresciau.4c00045
ACS Meas. Sci. Au 2024, 4, 577−584

centrifugation at 1000 rpm for 3 min at room temperature, washed with DPBS, and resuspended in 1640 medium. Equal amounts of these cells (9×10^5 cells) in 600 μL of 1640 medium were incubated with Gal-4-F-2-Cl, ROS-3-F, or a mixture of Gal-4-F-2-Cl and ROS-3-F at 37 °C for 18 h. After that, the samples were centrifuged at 5000 rpm for 5 min, and the supernatant (containing 10% D_2O and 20 μM NaTFA) was analyzed by ^{19}F NMR. For dynamic analysis of different senescence-associated biomarkers, L-02 cells treated with DOX (200 nM) for varied days (1, 2, 3, 4, 5, and 6 days) and L-02 cells without DOX treatment were collected by centrifugation, washed with DPBS, and resuspended in 1640 culture medium. Same numbers of these cells (9×10^5 cells) in 600 μL of 1640 medium were, respectively, incubated with Gal-4-F-2-Cl, ROS-3-F, or a mixture of Gal-4-F-2-Cl and ROS-3-F at 37 °C for 18 h. The concentration of these two probes was 400 μM. After that, the samples were centrifuged at 5000 rpm for 5 min, and the supernatant (containing 10% D_2O and 20 μM NaTFA) was analyzed by ^{19}F NMR.

RESULTS AND DISCUSSION

To ensure simultaneous detection of different senescence biomarkers, the activable ^{19}F NMR senoprobes must provide different ^{19}F NMR signals both before and after response to their targets. For this purpose, we first selected fluorobenzene (2-chloro-4-fluorophenol and 3-fluorophenol) as the backbone because the deshielding effect of the benzene ring is very sensitive to the electronic properties (electron-donating or electron-withdrawing) of the substituent. Next, galactose and borate ester were introduced and covalently conjugated to the molecular structure of the backbones as the recognition group toward β-gal and ROS, respectively, yielding the final activatable ^{19}F NMR probes, namely, Gal-4-F-2-Cl and ROS-3-F (Scheme S1). The obtained synthesis and spectral characterizations including ^{1}H NMR, ^{13}C NMR, and ^{19}F NMR are demonstrated in the Experimental section and in Figures S1–S8.

With these probes in hand, we first evaluated their reactivity to the targets by HPLC. Upon addition of β-gal, the peak at the retention time of 14.6 min corresponding to Gal-4-F-2-Cl was gradually decreased over time (Figures 2A and S9A), whereas a new peak at 21.9 min was detected and intensified, which was corresponded to 2-chloro-4-fluorophenol (4-F-2-Cl-OH), the product of enzymatic reaction, confirming the response of Gal-4-F-2-Cl toward β-gal. In parallel, the reactivity of ROS-3-F with ROS was studied. Upon treatment with H_2O_2, the peak at 17.9 min corresponding to ROS-3-F was dramatically decreased, and a new peak appearing at 19.9 min was found in a time-dependent manner (Figures 2B and S9B), which was ascribed to the product, 3-fluorophenol (3-F-OH for short). To further prove the reactivity, UV–vis absorbance spectra of the two probes were collected before and after treatment. The maximum absorption of Gal-4-F-2-Cl showed a slight red shift from 276 to 281 nm after treatment with β-gal, whereas a blue shift from 268 to 267 nm was observed after ROS-3-F was treated with H_2O_2 (Figure S10). Taken together, these results proved that Gal-4-F-2-Cl and ROS-3-F had good reactivity to the corresponding targets.

Next, we wondered whether these reactions could lead to changes in the ^{19}F NMR chemical shifts of these probes for target analysis. Prior to this test, the stability of the two probes was assessed. Intriguingly, no obvious changes in the ^{19}F chemical shift were noticed after 7 day storage or under different pH conditions (Figures S11 and S12). Subsequently, these probes were separately incubated with β-gal and H_2O_2 under the same conditions as those for HPLC analysis,

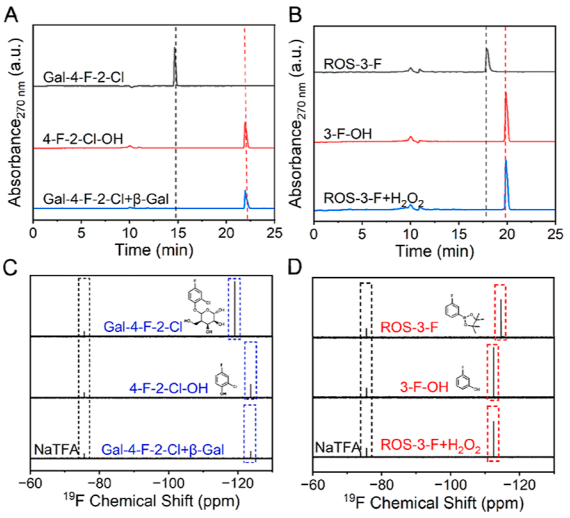

Figure 2. Reactivity studies. (A) HPLC profiles of Gal-4-F-2-Cl (400 μM) before and after incubation with β-gal (0.1 U/mL) for 3 h. (B) HPLC profiles of ROS-3-F (400 μM) before and after incubation with H_2O_2 (1 mM) for 3 h. (C,D) Corresponding ^{19}F NMR spectra of samples from panels (A,B). The gray dotted frame indicates the chemical shift of NaTFA (internal standard). The blue dotted frame indicates the chemical shift of Gal-4-F-2-Cl and its reaction product (4-F-2-Cl-OH). The red dotted frame indicates the chemical shift of ROS-3-F and 3-F-OH.

followed by ^{19}F NMR examinations. Meanwhile, sodium trifluoroacetate (NaTFA) was added as the reference standard for quantitative analysis. For the case of Gal-4-F-2-Cl, a sharp peak at −119.2 ppm was detected in the ^{19}F NMR spectrum without β-gal, and the intensity of this peak was gradually decreased over time upon reaction with β-gal and disappeared after 3 h, coupled with the appearance of a new peak at −123.0 ppm (Figures 2C and S13A), ascribable to the hydrolytic product 4-F-2-Cl-OH. Of note, there was 3.8 ppm of difference in ^{19}F NMR chemical shifts between Gal-4-F-2-Cl and 4-F-2-Cl-OH, which was sufficient to differentiate them by ^{19}F NMR. Likewise, a change of the ^{19}F chemical shift from −114.7 (ROS-3-F) to −112.4 ppm (3-F-OH) was detected when ROS-3-F was treated with H_2O_2 (Figures 2D and S13B).

Given the good reactivity of these probes, we proceeded to assess their selectivity. Specifically, the ^{19}F NMR spectra of Gal-4-F-2-Cl and ROS-3-F were recorded in the presence of different common bioactive substances including Fe^{2+}, Fe^{3+}, Cu^{2+}, carbonic anhydrases, lysozyme, carbonic cysteine, and glutathione (Figure 3A,B). Impressively, no changes in the ^{19}F chemical shift of ether Gal-4-F-2-Cl or ROS-3-F were noticed in the presence of any of these substances. In sharp contrast, the disappearance of peaks of these two probes, yet the appearance of the peaks of their reaction products, was observed in the presence of β-gal or ROS under the same conditions, indicating their target-specified reactivity. Moreover, we investigated whether these activatable probes could be used for the simultaneous detection of β-gal and ROS. A mixture of Gal-4-F-2-Cl and ROS-3-F was subjected to β-gal, H_2O_2, and the coexistence of β-gal and H_2O_2, respectively, followed by ^{19}F NMR analysis. Intriguingly, the target-triggered reactions of Gal-4-F-2-Cl and ROS-3-F were not influenced. When β-gal was present only in the reaction system, for instance, the peak corresponding to the reaction product 4-F-2-Cl-OH at −123.0 ppm was detected, while we

https://doi.org/10.1021/acsmeasuresciau.4c00045
ACS Meas. Sci. Au 2024, 4, 577–584

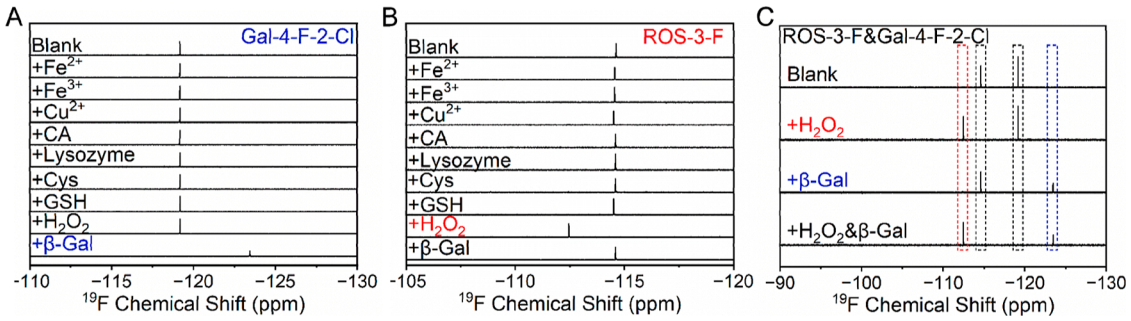

Figure 3. Selectivity evaluations. (A) ^{19}F NMR spectra of Gal-4-F-2-Cl (400 μM) after treatment with Fe^{2+} (1 mM), Fe^{3+}(1 mM), Cu^{2+}(1 mM), carbonic anhydrases (CA, 1 U/mL), lysozyme (1 U/mL), carbonic cysteine (Cys, 1 mM), glutathione (GSH, 1 mM), hydrogen peroxide (H_2O_2, 1 mM), and β-gal (0.1 U/mL) for 3 h. (B) ^{19}F NMR spectra of ROS-3-F (400 μM) treated with Fe^{2+} (1 mM), Fe^{3+}(1 mM), Cu^{2+}(1 mM), carbonic anhydrases (CA, 1 U/mL), lysozyme (1 U/mL), carbonic cysteine (Cys, 1 mM), glutathione (GSH, 1 mM), hydrogen peroxide (H_2O_2, 1 mM), and β-gal (0.1 U/mL) for 3 h. (C) ^{19}F NMR spectra of the mixture of Gal-4-F-2-Cl (400 μM) and ROS-3-F (400 μM) after treatment with H_2O_2 (1 mM), β-gal (0.1 U/mL), and a mixture of H_2O_2 (1 mM) and β-gal (0.1 U/mL) for 3 h. The black dotted frame indicates the chemical shift of Gal-4-F-2-Cl (right dotted frame) and ROS-3-F (left dotted frame). The blue dotted frame and red dotted frame indicate the chemical shift of 4-F-2-Cl-OH and 3-F-OH (reaction products of Gal-4-F-2-Cl and ROS-3-F with their targets), respectively.

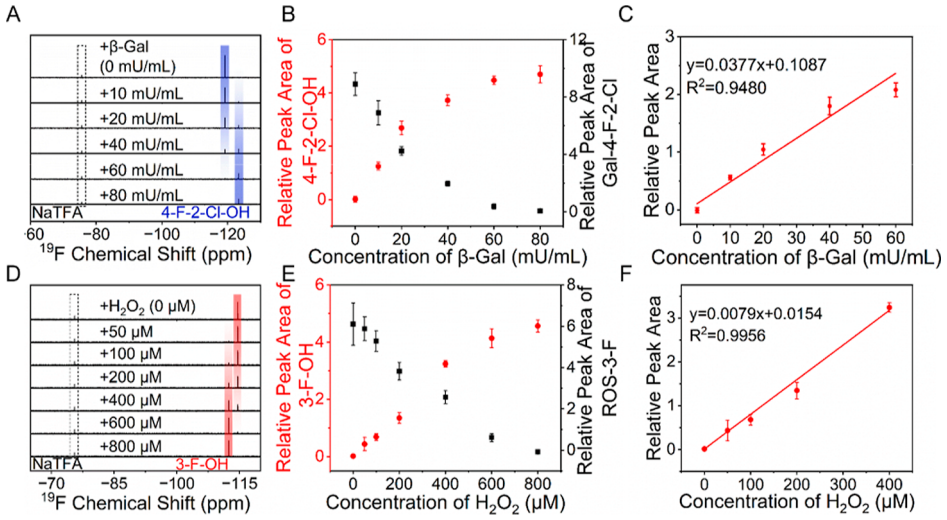

Figure 4. Quantitative studies. (A) ^{19}F NMR spectra of Gal-4-F-2-Cl (400 μM) after treatment with β-gal at various concentrations (0−80 mU/mL) for 3 h. The blue bands indicate the chemical shift of Gal-4-F-2-Cl (left band) and its reaction product (4-F-2-Cl-OH, right band). (B) Relative peak area of Gal-4-F-2-Cl and its reaction product upon mixing of Gal-4-F-2-Cl with β-gal at 0−80 mU/mL for 3 h. The peak area of NaTFA (the internal standard) was normalized to 1. (C) Corresponding linear fittings of this reaction. (D) ^{19}F NMR spectra of ROS-3-F (400 μM) after treatment with H_2O_2 at 0−800 μM for 3 h. The red bands indicate the chemical shift of ROS-3-F (right band) and its reaction product (3-F-OH, left band). (E) Relative peak area of ROS-3-F and the reaction product upon mixing of ROS-3-F with different concentrations of H_2O_2. (F) Corresponding linear fittings of this reaction. The experiments were performed in triplicate, and the data are shown as mean ± SD.

did not observe the peak corresponding to the reaction product 3-F-OH at −112.4 ppm. A similar phenomenon occurred for the case of H_2O_2 alone. On the other hand, such reactions of these two probes and the corresponding changes of ^{19}F chemical shifts took place when β-gal and H_2O_2 were coexisted in the reaction system (Figure 3C), without the formation of new peaks or obvious difference in chemical shifts as compared to the cases of single-marker detection. These results collectively provided strong support for the potent selectivity of these probes and the potential for simultaneous monitoring of β-gal and ROS in senescent cells.

Since ^{19}F NMR is a robust technique to quantify the concentration of samples, we next investigated the feasibility of using these probes for the quantitative measurement of β-gal and H_2O_2. The correlation between the ^{19}F NMR signal intensity of the reaction product and the target concentration was explored. As shown in Figure 4, the ^{19}F NMR signal intensity of the reaction product was gradually enhanced with the increase of the target concentration. With these two probes, the limit of detection for β-gal and H_2O_2 was calculated to be 4.5 mU/mL and 4.4 μM, respectively, allowing them to detect these two biomarkers in biological systems.[39,40]

Encouraged by the above promising results, we embarked on an exploration of the capacity of these activatable ^{19}F NMR probes for monitoring β-gal and ROS in senescent cells. To do this exploration, we first established chemotherapy-induced cellular senescence models with four different cells as the sources, including two normal cell lines (L-02 and HEK293T) and two cancer cell lines (A549 and PC-3) and with doxorubicin (DOX) as the model inducer. The successful construction of these cellular senescence models was verified via different characterizations. Given that β-gal was the gold standard for the identification of senescent cells, we performed

https://doi.org/10.1021/acsmeasuresciau.4c00045
ACS Meas. Sci. Au 2024, 4, 577−584

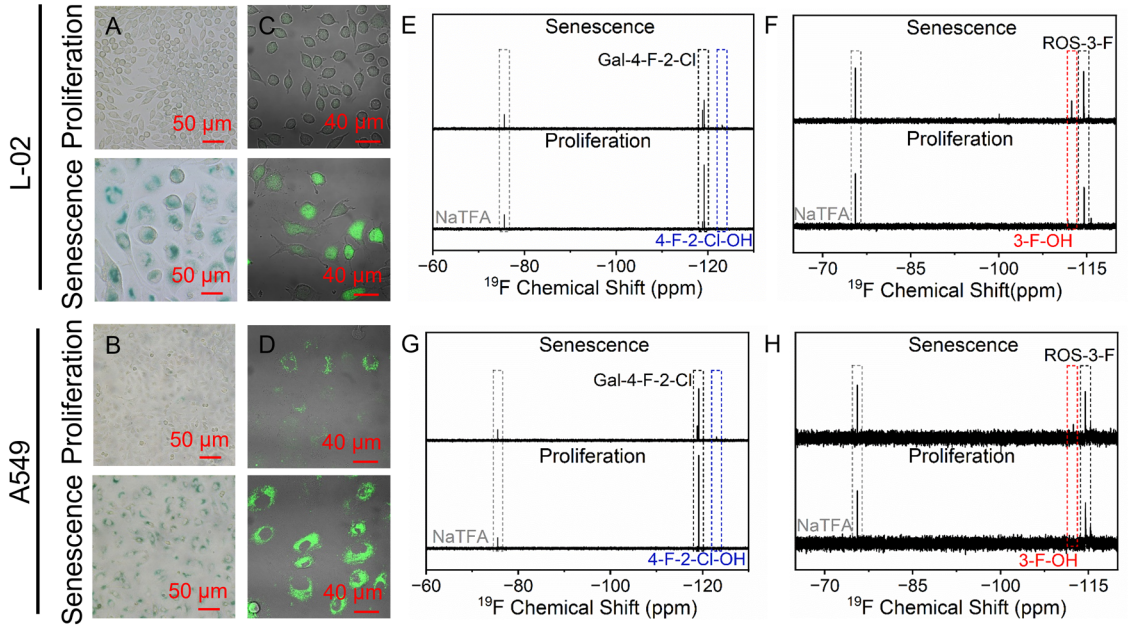

Figure 5. Evaluations of the capability of the proposed activatable multiplexed ^{19}F NMR senoprobes for the detection of intracellular β-gal and ROS in senescent cells. (A,C) SA-β-gal staining and H_2DCFDA staining of proliferating L-02 cells and DOX-induced senescent L-02 cells. (B,D) SA-β-gal staining and H_2DCFDA staining of proliferating A549 and DOX-induced senescent A549 cells. (E,F) ^{19}F NMR spectra of (E) Gal-4-F-2-Cl (400 μM) and (F) ROS-3-F (400 μM) after incubation with proliferating and senescent L-02 cells for 18 h, respectively. (G,H) ^{19}F NMR spectra of (G) Gal-4-F-2-Cl (400 μM) and (H) ROS-3-F (400 μM) after incubation with proliferating and senescent A549 cells for 18 h, respectively. The gray dotted frame indicates the chemical shift of NaTFA (internal standard). The black dotted frame indicates the chemical shift of Gal-4-F-2-Cl and ROS-3-F. The blue dotted frame and red dotted frame indicate the chemical shift of 4-F-2-Cl-OH and 3-F-OH (reaction products of Gal-4-F-2-Cl and ROS-3-F with their targets), respectively.

SA-β-gal staining first. After DOX treatment, all these cells showed evident SA-β-gal positive staining compared to nontreated groups (Figures 5A,B, S14, and S15). Other hallmarks of senescence including increased DNA damage, enlargement in the cell volume, and elevated ROS levels were also observed in all DOX-treated cells when compared to their proliferating control groups, further proving the successful introduction of cellular senescence (Figures 5C,D and S14–S17).

Afterward, the potential of the proposed activatable ^{19}F NMR probes for the detection of intracellular SA-β-gal and ROS in different senescent cells was evaluated. Prior to NMR measurements, the cytotoxicity of Gal-4-F-2-Cl and ROS-3-F in these cell lines was first examined using the Alamar blue assay. Impressively, the results showed that these two probes exhibited good biocompatibility without causing significant cell death in both proliferating and senescent states at a concentration of up to 800 μM (Figures S18 and S19). Next, different types of senescent cells and the corresponding proliferating controls were separately treated with Gal-4-F-2-Cl and ROS-3-F, followed by ^{19}F NMR analysis. As we expected, a target-triggered specific ^{19}F chemical shift was observed, consistent with the results obtained from solution-phase analysis. For instance, treatment of senescent L-02 cells with Gal-4-F-2-Cl led to a decreased ^{19}F NMR signal intensity at −119.2 ppm and the appearance of a new peak at −123.0 ppm (Figure 5E). However, such changes were not observed in proliferating cells. Similarly, we noticed an obvious ^{19}F NMR peak at −112.4 ppm in ROS-3-F-treated senescent L-02 cells but not in proliferating cells (Figure 5F), suggesting that the ROS level was increased in senescent cells, which was well consistent with the above ROS staining results. Furthermore, the ^{19}F NMR measurements were conducted in other three senescent cell types including A549, PC-3, and HEK293T cells, which were widely employed for cellular senescence studies.[18,20] Results demonstrated that Gal-4-F-2-Cl and ROS-3-F could also be used to monitor the level of intracellular SA-β-gal and ROS in these cells upon cellular senescence (Figures 5G,H, S20, and S21). Please note that the ^{19}F NMR signal changes were varied among different cell types, presumably due to the heterogeneous nature of senescence.

It has been increasingly recognized that simultaneous monitoring of different senescence-associated biomarkers is crucial not only for improving the detection accuracy toward cellular senescence but also for better understanding the molecular signature of this biological process.[16−20] Motivated by the above promising results, we proceeded to investigate the potential of these activatable ^{19}F NMR probes for the simultaneous analysis of β-gal and ROS in four types of senescent cells. A mixture of Gal-4-F-2-Cl and ROS-3-F was incubated with DOX-induced senescent cells and subjected to ^{19}F NMR measurement. For comparison, the corresponding proliferating cells were studied as the reference. As shown in Figure 6, the ^{19}F NMR peaks at −123.0 and −112.4 ppm, assigned to the two reaction products, appeared only in the cells with DOX treatment, regardless of the cell type, revealing the promise of the proposed multiplexed ^{19}F NMR strategy for the assessment of the changes of different senescence-related biomarkers among different types of cell sources.

Aside from cell type, stress duration is another important factor contributing to the high heterogeneity of cellular senescence. In this regard, we additionally tested the potential of these probes for the dynamic analysis of these two markers in cells upon stress. As a proof-of-concept illustration, the tests

https://doi.org/10.1021/acsmeasuresciau.4c00045
ACS Meas. Sci. Au 2024, 4, 577−584

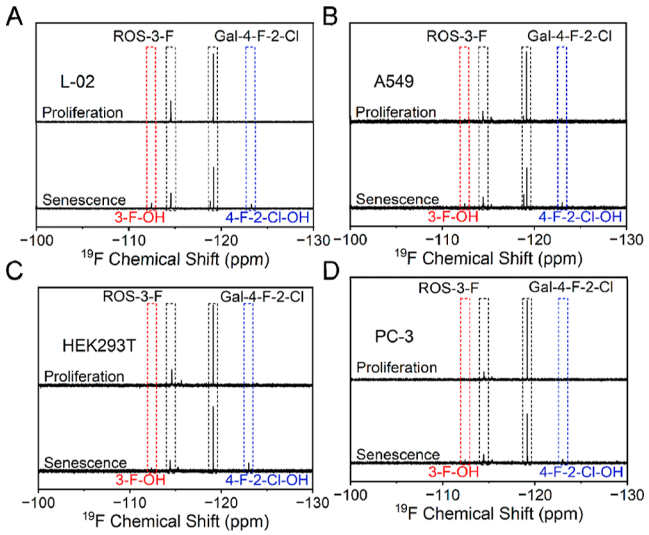

Figure 6. Studies on the capability of the activatable multiplexed ^{19}F NMR senoprobes for the simultaneous detection of β-gal and ROS in different types of senescent cells. ^{19}F NMR of the samples after incubation of a mixture of Gal-4-F-2-Cl (400 μM) and ROS-3-F (400 μM) with (A) proliferating and senescent L-02 cells, (B) proliferating and senescent A549 cells, (C) proliferating and senescent HEK293T, and (D) proliferating and senescent PC-3 cells for 18 h. The black dotted frame indicates the chemical shift of Gal-4-F-2-Cl and ROS-3-F. The blue dotted frame and red dotted frame indicate the chemical shift of 4-F-2-Cl-OH and 3-F-OH (the reaction products of Gal-4-F-2-Cl and ROS-3-F with their targets), respectively.

were carried out in senescent L-02 cells with varied stimulating durations. Specifically, L-02 cells were treated with DOX for different periods of time and then subjected to ^{19}F NMR measurement after incubation with Gal-4-F-2-Cl and ROS-3-F, respectively. As seen in Figure 7A, the ^{19}F NMR peak at −123.0 ppm, corresponding to the product after reaction with intracellular SA-β-gal, was observed on day 3 after stimulation with DOX, indicating that the level of β-gal was substantially elevated. On the other hand, the ^{19}F NMR peak at −112.4 ppm, which was ascribable to the product after reaction with intracellular ROS, appeared on day 2 (Figure 7B), revealing the heterogeneous changes of these two markers during cellular senescence. With the increase of DOX-stimulation time, the signal intensity of ^{19}F NMR at both −123.0 and −112.4 ppm increased remarkably, suggesting the accumulation of intracellular SA-β-gal and ROS. More importantly, consistent results were obtained when Gal-4-F-2-Cl and ROS-3-F were coexisted (Figure 7C). Collectively, these findings highlighted the promise of our activatable multiplexed ^{19}F NMR probes for the dynamic monitoring of different senescence-associated biomarkers during cellular senescence.

CONCLUSIONS

In summary, we have presented a ^{19}F barcoding strategy for the quantitative measurement and dynamic monitoring of senescence-associated biomarkers based on the ^{19}F NMR technique. Our strategy is conceptually and operationally distinctive from currently studied senescence-detection approaches. The fingerprint and quantifiable ^{19}F chemical shifts were applied as the signal output, making it possible to overcome the spectral overlapping issue in traditional optical imaging methods in multitarget analysis and thereby enhance detection throughput. Moreover, the extremely low abundance of the F element in organism allows for dramatically decreased background interference, leading to improved analytical accuracy. Proof-of-concept studies have been conducted, and two activatable multiplexed ^{19}F NMR molecular probes have been designed and synthesized, which separately target two major senescence-associated biomarkers, β-gal and ROS. The potential of these two probes has been investigated for dynamical and quantitative assessment of the changes of these biomarkers in different types of cells undergoing cellular senescence. Results showed that they could specifically respond to their own target and generate different new chemical entities with different ^{19}F chemical shifts from the initial probes, enabling sensitive and quantitative assessment of β-gal and ROS in different cell models without inducing significant cytotoxicity. More impressively, no signal overlap was observed, which was ascribed to the remarkable difference in the ^{19}F chemical shifts between the initial probes and the reaction products, further contributing to the simultaneous analysis of β-gal and ROS in senescent cells. Despite these promising results, this study has limitations. Since cellular senescence is a dynamic and heterogeneous biological process, different types of ^{19}F NMR senoprobes targeting other senescence-related markers are highly needed in future studies

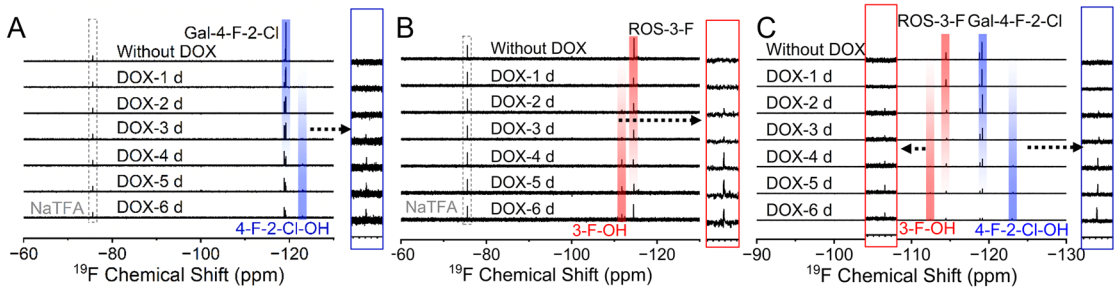

Figure 7. Studies on the capability of the proposed activatable multiplexed ^{19}F NMR senoprobes for dynamic monitoring of different biomarkers in senescent cells. (A) ^{19}F NMR spectra of the as-obtained samples after incubation of Gal-4-F-2-Cl (400 μM) with L-02 cells upon inducing by DOX for indicated periods of time. (B) ^{19}F NMR spectra of the as-obtained samples after incubation of ROS-3-F (400 μM) with L-02 cells upon inducing by DOX for indicated periods of time. (C) ^{19}F NMR spectra of the as-obtained samples after incubation of a mixture of Gal-4-F-2-Cl (400 μM) and ROS-3-F (400 μM) with L-02 cells upon inducing by DOX for indicated periods of time. The gray dotted frame indicates the chemical shift of NaTFA (internal standard). The blue bands indicate the chemical shift of Gal-4-F-2-Cl (left band) and 4-F-2-Cl-OH (right band). The red bands indicate the chemical shift of 3-F-OH (left band) and ROS-3-F (right band). The red frame and the blue frame indicate local amplification for better observation of the peaks of 3-F-OH and 4-F-2-Cl-OH.

https://doi.org/10.1021/acsmeasuresciau.4c00045
ACS Meas. Sci. Au 2024, 4, 577−584

in order to gain more insights into the molecular mechanism and mapping of cellular senescence derived from different cell sources and stress types. It is also important to perform in-depth investigations on the potential of these senoprobes for senescence detection in vivo, which would benefit us to further depict the roles of cellular senescence in aging and the development of age-related diseases. Besides, several other aspects, such as pharmacokinetics, biodistribution, biodegradation, and toxicological effects of the engineered probes, demand careful assessments. Overall, we expect this work to provide valuable molecular tools toward cellular senescence and lay the foundation to create an arsenal of senoprobes for promoting further advances in the field of cellular senescence.

■ ASSOCIATED CONTENT

Supporting Information

The Supporting Information is available free of charge at https://pubs.acs.org/doi/10.1021/acsmeasuresciau.4c00045.

Detailed synthetic procedures and spectral characterizations of the probes and intermediates, UV−vis absorption spectra of Gal-4-F-2-Cl and ROS-3-F in response to their targets, characterizations of senescent L-02, A549, HEK293T, and PC-3 cells, cytotoxicity evaluation of Gal-4-F-2-Cl and ROS-3-F, reactivity kinetics and stability tests of these probes, and ^{19}F NMR spectra of probes after incubation with senescent HEK293T cells, senescent PC-3 cells, and the corresponding proliferating control cells (PDF)

■ AUTHOR INFORMATION

Corresponding Authors

Jili Li − *Molecular Science and Biomedicine Laboratory (MBL), State Key Laboratory of Chemo/Biosensing and Chemometrics, College of Chemistry and Chemical Engineering, Aptamer Engineering Center of Hunan Province, Hunan University, Changsha, Hunan 410082, China*; Email: lijili@hnu.edu.cn

Yanlan Liu − *Molecular Science and Biomedicine Laboratory (MBL), State Key Laboratory of Chemo/Biosensing and Chemometrics, College of Chemistry and Chemical Engineering, Aptamer Engineering Center of Hunan Province, Hunan University, Changsha, Hunan 410082, China*; orcid.org/0000-0002-1757-6810; Email: ylliu@hnu.edu.cn

Authors

Jian Wang − *Molecular Science and Biomedicine Laboratory (MBL), State Key Laboratory of Chemo/Biosensing and Chemometrics, College of Chemistry and Chemical Engineering, Aptamer Engineering Center of Hunan Province, Hunan University, Changsha, Hunan 410082, China*

Donghui Hong − *Molecular Science and Biomedicine Laboratory (MBL), State Key Laboratory of Chemo/Biosensing and Chemometrics, College of Chemistry and Chemical Engineering, Aptamer Engineering Center of Hunan Province, Hunan University, Changsha, Hunan 410082, China*

Linlin Wang − *Molecular Science and Biomedicine Laboratory (MBL), State Key Laboratory of Chemo/Biosensing and Chemometrics, College of Chemistry and Chemical Engineering, Aptamer Engineering Center of Hunan Province, Hunan University, Changsha, Hunan 410082, China*

Yuqi Xie − *Molecular Science and Biomedicine Laboratory (MBL), State Key Laboratory of Chemo/Biosensing and Chemometrics, College of Chemistry and Chemical Engineering, Aptamer Engineering Center of Hunan Province, Hunan University, Changsha, Hunan 410082, China*

Jun Da − *Molecular Science and Biomedicine Laboratory (MBL), State Key Laboratory of Chemo/Biosensing and Chemometrics, College of Chemistry and Chemical Engineering, Aptamer Engineering Center of Hunan Province, Hunan University, Changsha, Hunan 410082, China*

Complete contact information is available at: https://pubs.acs.org/10.1021/acsmeasuresciau.4c00045

Author Contributions

The manuscript was written through contributions of all authors. All authors have given approval to the final version of the manuscript. CRediT: **Jian Wang** conceptualization, data curation, formal analysis, writing - original draft; **Donghui Hong** data curation, formal analysis, investigation; **Jili Li** conceptualization, data curation, formal analysis, funding acquisition, writing - original draft; **Linlin Wang** data curation, formal analysis, software, validation; **Yuqi Xie** formal analysis, software, writing - review & editing; **Jun Da** formal analysis, writing - review & editing; **Yanlan Liu** conceptualization, formal analysis, funding acquisition, project administration, supervision, writing - review & editing.

Notes

The authors declare no competing financial interest.

■ ACKNOWLEDGMENTS

This work was supported by the National Key Research and Development Program of China (2020YFA0210802), the National Natural Science Foundation of China (NSFC22274044 and 21877031), the Science and Technology Innovation Program of Hunan Province (2023RC1037 and 2018RS3043), and the China Postdoctoral Science Foundation (2023M741119).

■ REFERENCES

(1) Muñoz-Espín, D.; Serrano, M. Cellular Senescence: From Physiology to Pathology. *Nat. Rev. Mol. Cell Biol.* **2014**, *15*, 482−496.

(2) Gorgoulis, V.; Adams, P. D.; Alimonti, A.; Bennett, D. C.; Bischof, O.; Bishop, C.; Campisi, J.; Collado, M.; Evangelou, K.; Ferbeyre, G.; Gil, J.; Hara, E.; Krizhanovsky, V.; Jurk, D.; Maier, A. B.; Narita, M.; Niedernhofer, L.; Passos, J. F.; Robbins, P. D.; Schmitt, C. A.; Sedivy, J.; Vougas, K.; von Zglinicki, T.; Zhou, D.; Serrano, M.; Demaria, M. Cellular Senescence: Defining a Path Forward. *Cell* **2019**, *179*, 813−827.

(3) Di Micco, R.; Krizhanovsky, V.; Baker, D.; d'Adda di Fagagna, F. Cellular Senescence in Ageing: From Mechanisms to Therapeutic Opportunities. *Nat. Rev. Mol. Cell Biol.* **2021**, *22*, 75−95.

(4) Taylor, R. C.; Cullen, S. P.; Martin, S. J. Apoptosis: Controlled Demolition at the Cellular Level. *Nat. Rev. Mol. Cell Biol.* **2008**, *9*, 231−241.

(5) Collado, M.; Serrano, M. Senescence in Tumours: Evidence from Mice and Humans. *Nat. Rev. Cancer* **2010**, *10*, 51−57.

(6) Nardella, C.; Clohessy, J. G.; Alimonti, A.; Pandolfi, P. P. Pro-Senescence Therapy for Cancer Treatment. *Nat. Rev. Cancer* **2011**, *11*, 503−511.

(7) Prasanna, P. G.; Citrin, D. E.; Hildesheim, J.; Ahmed, M. M.; Venkatachalam, S.; Riscuta, G.; Xi, D.; Zheng, G.; Deursen, J. V.; Goronzy, J.; Kron, S. J.; Anscher, M. S.; Sharpless, N. E.; Campisi, J.; Brown, S. L.; Niedernhofer, L. J.; O'Loghlen, A.; Georgakilas, A. G.; Paris, F.; Gius, D.; Gewirtz, D. A.; Schmitt, C. A.; Abazeed, M. E.; Kirkland, J. L.; Richmond, A.; Romesser, P. B.; Lowe, S. W.; Gil, J.; Mendonca, M. S.; Burma, S.; Zhou, D.; Coleman, C. N. Therapy-Induced Senescence: Opportunities to Improve Anticancer Therapy. *J. Natl. Cancer Inst.* **2021**, *113*, 1285−1298.
(8) Collado, M.; Blasco, M. A.; Serrano, M. Cellular Senescence in Cancer and Aging. *Cell* **2007**, *130*, 223−233.
(9) DePinho, R. A. The Age of Cancer. *Nature* **2000**, *408*, 248−254.
(10) Huang, W.; Hickson, L. J.; Eirin, A.; Kirkland, J. L.; Lerman, L. O. Cellular Senescence: The Good, the Bad and the Unknown. *Nat. Rev. Nephrol.* **2022**, *18*, 611−627.
(11) Gasek, N. S.; Kuchel, G. A.; Kirkland, J. L.; Xu, M. Strategies for Targeting Senescent Cells in Human Disease. *Nat. Aging* **2021**, *1*, 870−879.
(12) Kirschner, K.; Rattanavirotkul, N.; Quince, M. F.; Chandra, T. Functional heterogeneity in senescence. *Biochem. Soc. Trans.* **2020**, *48*, 765−773.
(13) Baker, A. G.; Hartono, M.; Ou, H. L.; Popov, A. B.; Brown, E. L.; Joseph, J.; Golinska, M.; González-Gualda, E.; Macias, D.; Ge, J. F.; Denholm, M.; Morsli, S.; Sanghera, C.; Else, T. R.; Greer, H. F.; Vernet, A.; Bohndiek, S. E.; Muñoz-Espín, D.; Fruk, L. An Indocyanine Green-Based Nanoprobe for *In Vivo* Detection of Cellular Senescence. *Angew. Chem., Int. Ed.* **2024**, *63*, No. e202404885.
(14) Li, J. L.; Xie, Y. Q.; Wang, J.; Wang, L. L.; Xia, Y. H.; Liu, Y. L.; Tan, W. H. Activatable and Self-Monitoring Hydrogen Sulfide-Based Molecular Senomorphics for Visualized Regulation of Cellular Senescence. *CCS Chem.* **2023**, *5*, 2897−2909.
(15) Lozano-Torres, B.; Blandez, J. F.; Galiana, I.; Garcia-Fernandez, A.; Alfonso, M.; Marcos, M. D.; Orzáez, M.; Sancenón, F.; Martínez-Máñez, R. Real-Time in Vivo Detection of Cellular Senescence Through the Controlled Release of the NIR Fluorescent Dye Nile Blue. *Angew. Chem., Int. Ed.* **2020**, *59*, 15152−15156.
(16) Gao, Y.; Hu, Y.; Liu, Q.; Li, X.; Li, X.; Kim, C. Y.; James, T. D.; Li, J.; Chen, X.; Guo, Y. Two-Dimensional Design Strategy to Construct Smart Fluorescent Probes for the Precise Tracking of Senescence. *Angew. Chem., Int. Ed.* **2021**, *60*, 10756−10765.
(17) Zhou, L.; Zhang, X.; Dong, Y.; Pan, Y.; Li, J.; Zang, Y.; Li, X. A Tandemly Activated Fluorescence Probe for Detecting Senescent Cells with Improved Selectivity by Targeting a Biomarker Combination. *ACS Sens.* **2022**, *7*, 1958−1966.
(18) Li, J.; Wang, L.; Luo, X.; Xia, Y.; Xie, Y.; Liu, Y.; Tan, W. Dual-Parameter Recognition-Directed Design of the Activatable Fluorescence Probe for Precise Imaging of Cellular Senescence. *Anal. Chem.* **2023**, *95*, 3996−4004.
(19) Liu, H. H.; Lv, R. D.; Song, F. X.; Yang, Y. Q.; Zhang, F.; Xin, L. T.; Zhang, P.; Zhang, Q.; Ding, C. F. A Near-IR Ratiometric Fluorescent Probe for the Precise Tracking of Senescence: A Multidimensional Sensing Assay of Biomarkers in Cell Senescence Pathways. *Chem. Sci.* **2024**, *15*, 5681−5693.
(20) Wang, L. L.; Li, J. L.; Zhao, Z. H.; Xia, Y. H.; Xie, Y. Q.; Hong, D. H.; Liu, Y. L.; Tan, W. H. Aptamer Conjugate-Based Ratiometric Fluorescent Probe for Precise Imaging of Therapy-Induced Cancer Senescence. *Anal. Chem.* **2024**, *96*, 154−162.
(21) Shi, D.; Liu, W.; Gao, Y.; Li, X.; Huang, Y.; Li, X.; James, T. D.; Guo, Y.; Li, J. Photoactivatable Senolysis with Single-Cell Resolution Delays Aging. *Nat. Aging* **2023**, *3*, 297−312.
(22) Tanaka, H.; Sugawara, S.; Tanaka, Y.; Loo, T. M.; Tachibana, R.; Abe, A.; Kamiya, M.; Urano, Y.; Takahashi, A. Dipeptidylpeptidase-4-Targeted Activatable Fluorescent Probes Visualize Senescent Cells. *Cancer Sci.* **2024**, *115*, 2762−2773.
(23) Rojas-Vázquez, S.; Lozano-Torres, B.; García-Fernández, A.; Galiana, I.; Perez-Villalba, A.; Martí-Rodrigo, P.; Palop, M. J.; Domínguez, M.; Orzáez, M.; Sancenón, F.; Blandez, J. F.; Fariñas, I.; Martínez-Máñez, R. A Renal Clearable Fluorogenic Probe for in Vivo β-Galactosidase Activity Detection during Aging and Senolysis. *Nat. Commun.* **2024**, *15*, 775.
(24) Li, J.; Bi, Z.; Wang, L.; Xia, Y.; Xie, Y.; Liu, Y. Recent Advances in Strategies for Imaging Detection and Intervention of Cellular Senescence. *ChemBioChem* **2023**, *24*, No. e202200364.
(25) García-Fleitas, J.; García-Fernández, A.; Martí-Centelles, V.; Sancenón, F.; Bernardos, A.; Martínez-Máñez, R. Chemical Strategies for the Detection and Elimination of Senescent Cells. *Acc. Chem. Res.* **2024**, *57*, 1238−1253.
(26) He, Z. R.; Xu, K.; Li, Y. M.; Gao, H.; Miao, T. T.; Zhao, R.; Huang, Y. Y. Molecularly Targeted Fluorescent Sensors for Visualizing and Tracking Cellular Senescence. *Biosensors* **2023**, *13*, 838.
(27) Li, A.; Luo, X. J.; Chen, D. X.; Li, L. X.; Lin, H. Y.; Gao, J. H. Small Molecule Probes for ^{19}F Magnetic Resonance Imaging. *Anal. Chem.* **2023**, *95*, 70−82.
(28) Chen, H.; Viel, S.; Ziarelli, F.; Peng, L. ^{19}F-NMR: a valuable tool for studying biological events. *Chem. Soc. Rev.* **2013**, *42*, 7971−7982.
(29) Cui, C. Y.; Li, B.; Su, X. C. Real-Time Monitoring of the Level and Activity of Intracellular Glutathione in Live Cells at Atomic Resolution by ^{19}F-NMR. *ACS Cent. Sci.* **2023**, *9*, 1623−1632.
(30) Yamaguchi, K.; Ueki, R.; Nonaka, H.; Sugihara, F.; Matsuda, T.; Sando, S. Design of Chemical Shift-Switching^{19}F Magnetic Resonance Imaging Probe for Specific Detection of Human Monoamine Oxidase A. *J. Am. Chem. Soc.* **2011**, *133*, 14208−14211.
(31) Chen, S. Z.; Xiao, L.; Li, Y.; Qiu, M. S.; Yuan, Y. P.; Zhou, R.; Li, C. G.; Zhang, L.; Jiang, Z. X.; Liu, M. L.; Zhou, X. In Vivo Nitroreductase Imaging via Fluorescence and Chemical Shift Dependent ^{19}F-NMR. *Angew. Chem., Int. Ed.* **2022**, *61*, No. e202213495.
(32) Yuan, S.; Zhu, Y.; Dai, Y.; Wang, Y.; Jin, D.; Liu, M.; Tang, L.; Arnesano, F.; Natile, G.; Liu, Y. ^{19}F-NMR Allows the Investigation of the Fate of Platinum (IV) Prodrugs in Physiological Conditions. *Angew. Chem., Int. Ed.* **2022**, *61*, No. e202114250.
(33) Shusterman-Krush, R.; Tirukoti, N. D.; Bandela, A. K.; Avram, L.; Allouche-Arnon, H.; Cai, X.; Gibb, B. C.; Bar-Shir, A. Single Fluorinated Agent for Multiplexed 19F-MRI with Micromolar Detectability Based on Dynamic Exchange. *Angew. Chem., Int. Ed.* **2021**, *60*, 15405−15411.
(34) Fan, Y.; Chen, L.; Zheng, Y.; Li, A.; Lin, H.; Gao, J. Nanoparticle-Based Activatable MRI Probes for Disease Imaging and Monitoring. *Chem. Biomed. Imaging* **2023**, *1*, 192−204.
(35) Hu, Y.; Wang, Y.; Wen, X.; Pan, Y.; Cheng, X.; An, R.; Gao, G.; Chen, H.-Y.; Ye, D. Responsive Trimodal Probes for In Vivo Imaging of Liver Inflammation by Coassembly and GSH-Driven Disassembly. *Research* **2020**, *2020*, 4087069.
(36) Wu, T.; Liu, C.; Thamizhchelvan, A. M.; Fleischer, C.; Peng, X.; Liu, G.; Mao, H. Label-Free Chemically and Molecularly Selective Magnetic Resonance Imaging. *Chem. Biomed. Imaging* **2023**, *1*, 121−139.
(37) Xu, Z.; Liu, C.; Zhao, S.; Chen, S.; Zhao, Y. Molecular Sensors for NMR-Based Detection. *Chem. Rev.* **2019**, *119*, 195−230.
(38) Luo, X.; Kang, B.; Chi, X.; Xiong, H.; Chen, D.; Fan, Y.; Li, L.; Chen, L.; Li, A.; Gao, J.; Lin, H. ^{19}F Barcoding Enables Multiplex Detection of Biomarkers Associated with Organ Injury and Cancer. *Angew. Chem., Int. Ed.* **2022**, *61*, No. e202211189.
(39) Li, A.; Luo, X.; Li, L.; Chen, D.; Liu, X.; Yang, Z.; Yang, L.; Gao, J.; Lin, H. Activatable Multiplexed ^{19}F Magnetic Resonance Imaging Visualizes Reactive Oxygen and Nitrogen Species in Drug-Induced Acute Kidney Injury. *Anal. Chem.* **2021**, *93*, 16552−16561.
(40) Chen, J. A.; Guo, W.; Wang, Z. J.; Sun, N. N.; Pan, H. M.; Tan, J. H.; Ouyang, Z. R.; Fu, W.; Wang, Y. H.; Hu, W.; Gu, X. F. *In Vivo* Imaging of Senescent Vascular Cells in Atherosclerotic Mice Using a β-Galactosidase-Activatable Nanoprobe. *Anal. Chem.* **2020**, *92*, 12613−12621.

https://doi.org/10.1021/acsmeasuresciau.4c00045
ACS Meas. Sci. Au 2024, 4, 577−584